Propelled microprobes in turbulence

E. Calzavarini,[1,*] Y. X. Huang,[2] F. G. Schmitt,[3] and L. P. Wang[4]
[1]*Univ. Lille, Unité de Mécanique de Lille, UML EA 7512, F 59000 Lille, France*
[2]*State Key Laboratory of Marine Environmental Science, College of Ocean and Earth Sciences, Xiamen University, Xiamen 361102, People's Republic of China*
[3]*Univ. Lille, CNRS, Univ. Littoral Cote d'Opale, UMR 8187, Laboratoire d'Océanologie et de Géoscience, F 62930 Wimereux, France*
[4]*UM-SJTU Joint Institute, Shanghai JiaoTong University, Shanghai 200240, People's Republic of China*

(Received 2 February 2018; published 11 May 2018)

The temporal statistics of incompressible fluid velocity and passive scalar fields in developed turbulent conditions is investigated by means of direct numerical simulations along the trajectories of self-propelled pointlike probes drifting in a flow. Such probes are characterized by a propulsion velocity which is fixed in intensity and direction; however, like vessels in a flow they are continuously deviated on their intended course as the result of local sweeping of the fluid flow. The recorded time series by these moving probes represent the simplest realization of transect measurements in a fluid flow environment. We investigate the nontrivial combination of Lagrangian and Eulerian statistical properties displayed by the transect time series. We show that, as a result of the homogeneity and isotropy of the flow, the single-point acceleration statistics of the probes follows a predictable trend at varying the propulsion speed, a feature that is also present in the scalar time-derivative fluctuations. Further, by focusing on two-time statistics we characterize how the Lagrangian-to-Eulerian transition occurs at increasing the propulsion velocity. The analysis of intermittency of temporal increments highlights in a striking way the opposite trends displayed by the fluid velocity and passive scalars.

DOI: 10.1103/PhysRevFluids.3.054604

I. INTRODUCTION

In the oceanographic and meteorological context, field measurements of fluid velocity and scalar field intensities—such as temperature or concentrations of bio-geochemicals—are often performed by means of drifting instrumentations either self-propelled or pulled by moving vehicles. We refer, for instance, to the instrumentation used to perform the very first measurements of turbulence spectra in a open water flow, which was presented in the pioneering paper by Grant *et al.* [1], or to the vast literature on autonomous underwater vehicles (AUVs) [2,3] and their latest miniaturised versions (μAUVs for micro-AUVs) [4–6]. In all the above mentioned cases the probe positions always trace paths across the spatial domain which are the result of the interplay between the direction and intensity of motion imposed by the engine (or by the pulling system) [7] and the strength and orientation of the local sweeping of the fluid flow. Such paths are commonly denoted as *transects*. The shape of transect measurements reduces to a rectilinear one if the velocity impressed by the engine is overwhelming compared to the typical fluid velocity, while on the opposite limit, when the engine propulsion velocity is negligible, the transects become the trajectories of ideal fluid tracers. It is therefore clear that it is only in special limiting cases that transect measurements directly relate to the assessments

*enrico.calzavarini@polytech-lille.fr

that can be performed either in a fixed reference system (Eulerian frame) or in the system comoving with the flow (Lagrangian frame). Because it is natural and convenient to study flows either in the Eulerian or in the Lagrangian frames, there is the need to link the transect measurements to the known and thoroughly studied turbulence phenomenology in such frames.

The goal of the present study is to perform this task in a controlled and idealized setting, i.e., the case of an ensemble of pointlike inertia-less propelled probes (and so denoted as microprobes) which drift across a homogeneous and isotropic developed turbulent flow. In particular we would like to address the following key questions. How are the fluctuations of the fluid velocity and of a transported scalar quantity varying at changing the probe speed? Is it possible to grasp the functional dependence of the correlation time of the recorded signal versus the probe speed? What happens to velocity (scalar) time increments and to their higher statistical moments? In which conditions can we reasonably consider that the probe is sampling a frozen flow (scalar) field, which is the classical and often unstated assumption of oceanic cruise measurements? We will see that, despite the simple model of drifting microprobes under scrutiny, the statistical properties of measured quantities is far from being trivial.

The structure of the paper is as follows. First, we present the theoretical model system used, and we illustrate the numerical simulations and the main features of the database obtained by means of a numerical experiment. Second, we describe the data analysis and try, when possible, to substantiate it with analytical or phenomenological predictions and physical interpretation. The focus of the analysis section is both on single- and two-point statistics, in particular on fluid acceleration and velocity and on the scalar concentration field. In the conclusion we discuss the implications of our findings for real microprobe design and data interpretation and the future perspectives of this research.

II. MODELS AND METHODS

We consider a model system made of a set of pointlike, inertialess, self-propelled probes moving with the following equation of motion:

$$\dot{\boldsymbol{x}}_s(t) = \boldsymbol{u}(\boldsymbol{x}_s(t),t) + \boldsymbol{v}_s. \tag{1}$$

Here $\boldsymbol{u}(\boldsymbol{x}_s(t),t)$ denotes the fluid velocity at the position of the probe and $\boldsymbol{v}_s$ a given time-independent propulsion speed. Along these trajectories both the probe speed $\dot{\boldsymbol{x}}_s(t)$ and the local value of a scalar field, $\theta_s(t) \equiv \theta(\boldsymbol{x}_s(t),t)$, are recorded. The fluid environment in which the probes are placed evolves according to the Eulerian dynamics described by the incompressible Navier-Stokes equation for the velocity field $\boldsymbol{u}(\boldsymbol{x}(t),t)$ and by the advection-diffusion equation for the scalar $\theta(\boldsymbol{x}(t),t)$:

$$\partial_t \boldsymbol{u} + (\boldsymbol{u}\cdot\boldsymbol{\partial})\boldsymbol{u} = -\boldsymbol{\partial} p + \nu \boldsymbol{\partial}^2 \boldsymbol{u} + \boldsymbol{f}, \quad \boldsymbol{\partial}\cdot\boldsymbol{u} = 0, \tag{2}$$

$$\partial_t \theta + \boldsymbol{u}\cdot\boldsymbol{\partial}\theta = \kappa \boldsymbol{\partial}^2 \theta + \Phi. \tag{3}$$

The force to sustain the turbulent flow, $\boldsymbol{f}(\boldsymbol{x}(t),t)$, is divergence-less, acts only at large scales, provides a constant global power input, and is statistically homogeneous and isotropic. The scalar field is characterized by a unit Schmidt number, i.e., the scalar diffusivity, κ, has the same intensity as the kinematic viscosity, ν, of the advecting fluid. The scalar field is also sustained by a source term, $\Phi(\boldsymbol{x}(t),t)$, which acts at large scales and provides a constant global power input (i.e., scalar variance) in such a way to obtain a statistically stationary homogeneous and isotropic scalar turbulence. We remark that the scalar field has no feedback on the fluid flow; it is therefore said to be passive. The spatial domain is assumed to be tridimensional and cubic, of side L, with periodic boundary conditions for all fields. In these conditions the turbulent intensity is specified by a single dimensionless parameter, the Taylor-scale based Reynolds number, Re_λ, while the scalar turbulence is parametrized in terms of a Péclet number $\mathrm{Pe}_{\lambda_\theta}$.

The above described model, which is composed of Lagrangian (the probes) and Eulerian (the velocity and scalar fields) elements, can be numerically simulated. In this work the Eulerian

dynamics (2) is numerically computed on a Cartesian grid of N^3 points through a standard lattice Boltzmann equation solver based on a single-relaxation time scheme and a double-population algorithm [8]. Both the fluid external force and scalar source term are implemented through a combination of low wave-number sinusoidal functions with random phases controlled by independent Ornstein-Ulhenbeck processes, similar to Ref. [9] but with overall time dependent amplitudes in order to provide constant mechanical and scalar power to the system.

The numerically simulated turbulent flows are characterized by the globally averaged numbers $\mathrm{Re}_\lambda = 75$ and 125 and correspondingly $\mathrm{Pe}_{\lambda_\theta} = 43$ and 68. The values of all the relevant numerical and physical quantities of the simulated flows are reported for completeness in the Supplemental Material [10]. It is, however, important to note that in our simulations the spatial dissipative scales, the Kolmogorov scale, η, as well as the Bachelor scale, η_θ (which are here equal in magnitude), have been set to $\eta = \eta_\theta = 1.5\delta x$ with δx the numerical grid spacing. The time step of the simulation, δt, is instead nearly 300 times smaller than the dissipative timescale τ_η. This guarantees that the turbulent flow, both for the velocity and for the scalar field, is well resolved at all scales (see Supplemental Material [10] for a validation test).

The drifting probes evolution Eq. (1) is integrated in time via a second-order Adams-Bashforth algorithm with the same time stepping, δt, of the Eulerian algorithm. Trilinear interpolation is used to estimate the values of all the Eulerian quantities at the probe positions. The probe measurements, $\boldsymbol{u}$ and θ together with their gradients, are stored at regular intervals every $10\delta t$. Drifters have been divided into 21 groups, called probe families, corresponding to a discrete set of values of their propulsion speed intensity $|\boldsymbol{v}_s|$, which is here chosen in the range $[0,9u_\eta]$. There is an extra group of homogeneously distributed and fixed-in-space probes, which we call Eulerian probes. The members of each family differ from each other for the orientation of $\boldsymbol{v}_s$, which are taken homogeneously over the solid angle. This choice has been made just to obtain a faster convergence of the means. Therefore, in this work we denote with $\langle\cdots\rangle$ an average that is both over time and over an ensemble, where the ensembles are isotropic family of probes with equal $|\boldsymbol{v}_s|$. We track in time a total number of probes $N_p \simeq 2.2\times10^4$ at $\mathrm{Re}_\lambda = 75$ for a duration in large-eddy turnover units $T_e = L/u_{\mathrm{rms}}$ of $\sim 25\ T_e$ and $N_p \simeq 4.4\times10^4$ at $\mathrm{Re}_\lambda = 125$ for about 13.5 T_e. Because the observed phenomena at the two different Reynolds number are very similar, in this paper we sometime present only the results from the higher Reynolds and Péclet number dataset. However, we will comment whenever necessary on the expected and/or observed Reynolds and Péclet dependencies.

III. RESULTS

A visualization of three typical drifting probe trajectories over a time of $\sim 8T_e$ for different swimming velocity intensities is reported in Fig. 1. The shape of the curves (the transects) gets more and more straightened with the increase of the propulsion speed $\boldsymbol{v}_s$. From Eq. (1) it is indeed expected that a transect will be straight for $v_s \gg u_{\mathrm{rms}}$. At the considered Reynolds number ($\mathrm{Re}_\lambda = 125$) this corresponds to $v_s \gg u_{\mathrm{rms}} \simeq 10u_\eta$. From the same figure, which reports distances in term of the box size unit L, it is also evident that during the considered timespan the probes have crossed the box spatial domain several times. This is of course allowed by the implementations of periodic boundary conditions; however, the box crossing occurs over timescales long enough for the fluid to loose the past correlations, because $T_e \geqslant L/\sup(v_s)$.

We now look at the statistical features of the probe measurements. It is easy to verify that in a incompressible fluid flow $\boldsymbol{u}(\boldsymbol{x},t)$, as long as $\boldsymbol{v}_s$ is the same for a given set of probes, such probes do not form clusters. The argument goes as follows, we consider $\dot{\boldsymbol{x}}_s(t)$ as a field and take its divergence $\boldsymbol{\partial}\cdot\dot{\boldsymbol{x}}_s(t)$, this leads immediately to $\boldsymbol{\partial}\cdot\dot{\boldsymbol{x}}_s(t) = \boldsymbol{\partial}\cdot\boldsymbol{u} = 0$ due to the incompressibility of the carrying fluid flow. The absence of clustering for the probes has an immediate implication: the statistical moments of the fluid velocity and of the scalar measured by the probes are equal to the Lagrangian (L) and Eulerian (E) averages. Given the absence of the mean flow, i.e., $\langle\boldsymbol{u}(\boldsymbol{x},t)\rangle_t = 0\ \forall\boldsymbol{x}$ with $\langle\cdots\rangle_t$ denoting the time average, we deduce that $\langle(\dot{\boldsymbol{x}}_s - \boldsymbol{v}_s)^n\rangle_t = \langle\boldsymbol{u}_L^n\rangle_t = \langle\boldsymbol{u}_E^n\rangle_t$ for any given even integer

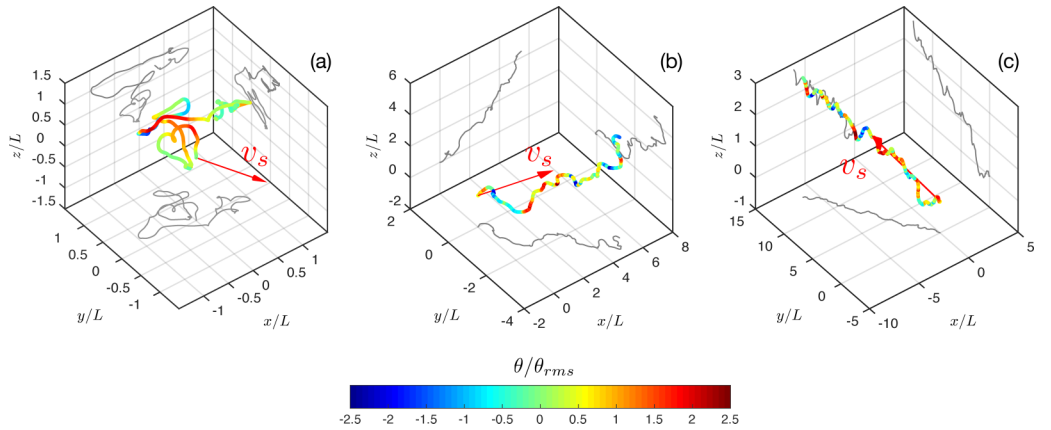

FIG. 1. Visualization of three drifting probes trajectories with different propulsion velocities in direction and intensity. The velocity intensity is (a) $v_s = 0.9\,u_\eta$, (b) $v_s = 4.3\,u_\eta$, and (c) $v_s = 9.0\,u_\eta$, while the orientation of the propulsion speed $\hat{\boldsymbol{v}}_s = \boldsymbol{v}_s/|\boldsymbol{v}_s|$ is denoted by the red arrow in each panel. $\mathrm{Re}_\lambda = 125$ for all cases. The trajectories shown here extend in time over about eight large-eddy-turnover time units (T_e). The box spatial units are expressed in term of the box size L.

n, while all odd values of n lead to zero moments. Similarly for the scalar, where the mean component $\langle\theta(\boldsymbol{x},t)\rangle_t = 0\ \forall \boldsymbol{x}$, one has $\langle\theta_s^n\rangle_t = \langle\theta_L^n\rangle_t = \langle\theta_E^n\rangle_t$ for even n and zero for the odd statistical moments.

A. Two time statistics: Infinitesimal time gaps

As we have observed above the statistical moments of the velocity and scalar recorded by the probes can be easily linked to the Eulerian and Lagrangian values. It is less evident, however, how to characterize the behavior of the moments of velocity and scalar differences in time given, for example, by their structure functions or spectra, as classically considered in fully developed turbulence. We begin this description by considering the limiting case of a difference over an infinitesimal time increment; this is equivalent to the study of the probe acceleration (or the fluid acceleration seen by the probe) and of the scalar time derivatives recorded by the probe.

1. Probe acceleration and scalar time derivative

The variance of the recorded fluid (or probe) acceleration as well as the scalar time derivative as a function of the propelling speed are reported in Figs. 2(a) and 2(b). It is evident that both quantities increase at increasing the propulsion speed. Furthermore, one can observe that the increase in the variance of the scalar derivative is much larger than that of the acceleration. What is the origin of such a behavior, and is it possible to account for it? In order to quantitatively understand this statistical signature, one has to consider that there is a strong similarity between the dynamics of pointlike drifting probes and the one of sub-Kolmogorov scale non-neutrally buoyant particles transported by the flow in the presence of gravity. The latter phenomenon has been recently addressed in Ref. [11], where it has been shown that for small inertial particles (bubbles or drops) vertical acceleration fluctuations were lower than horizontal acceleration fluctuations by a factor two, a factor which could be precisely connected to the statistics of local fluid flow gradients in a isotropic turbulent flow. Furthermore, it was observed that the dissipative velocity (u_η) was the relevant scale to describe the behavior of the acceleration variance at increasing the particle inertia. Likewise when one looks at acceleration of a small probe, $\ddot{\boldsymbol{x}}_s(t)$, the following relation holds:

$$\ddot{\boldsymbol{x}}_s(t) = D_t\boldsymbol{u}(\boldsymbol{x}_s(t),t) + (\boldsymbol{v}_s\cdot\boldsymbol{\partial})\boldsymbol{u}(\boldsymbol{x}_s(t),t), \tag{4}$$

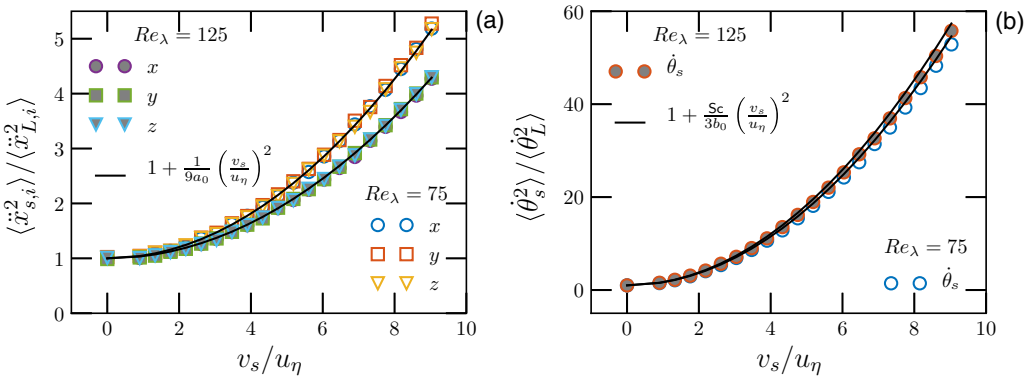

FIG. 2. (a) Variance of the probe acceleration, $\ddot{x}_{s,i}$ with index i denoting a Cartesian component ($i = x,y,z$), normalized by the variance of the fluid acceleration $\ddot{x}_{L,i}$ as a function of the propulsion velocity v_s. The continuous line corresponds to the prediction (5). (b) Variance of passive scalar time derivative and comparison with the prediction (6).

where $D_t(\bullet) = \partial_t(\bullet) + \boldsymbol{u} \cdot \boldsymbol{\partial}(\bullet)$ is the convective derivative along a fluid parcel or tracer. In homogeneous and isotropic turbulence it is safe to assume that the velocity gradients are independent from the material derivative, and along the lines of the derivation given in Ref. [11] one can show (see Supplemental Material [10] for a detailed derivation) that

$$\frac{\langle \ddot{x}_{s,i}^2 \rangle}{\langle \ddot{x}_{L,i}^2 \rangle} = 1 + \frac{1}{9a_0}\left(\frac{v_s}{u_\eta}\right)^2, \tag{5}$$

where a_0 is the so called Heisenberg-Yaglom (HY) constant, a quantity weakly dependent on Re_λ [12] and defined on the single component of the fluid acceleration $\ddot{x}_{L,i} = D_t u_i(\boldsymbol{x}_L(t),t)$ as $\langle \ddot{x}_{L,i}^2 \rangle = a_0 \epsilon/\tau_\eta$ (no summation over i implied). Therefore, the acceleration variance of a drifting probe is always larger than the one of fluid tracer. The above relation tells us also that the faster the propelling speed of the probe, the larger are the acceleration fluctuations experienced by the probe. The situation is analogous, although at much smaller scale, to the fluctuation due to atmospheric turbulence experienced on a airplane, where the intensity of fluctuations depends on its cruising speed [13]. Equation (5) is proven to be well verified by our numerical data; see Fig. 2(a).

Similarly to the fluid acceleration variance, the isotropy of the turbulent fluid and scalar flow requires that the time derivative of $\theta_s(t)$ follows

$$\frac{\langle \dot{\theta}_s^2 \rangle}{\langle \dot{\theta}_L^2 \rangle} = 1 + \frac{\mathrm{Sc}}{3b_0}\left(\frac{v_s}{u_\eta}\right)^2, \tag{6}$$

where b_0 is the scalar equivalent of the HY constant defined as $\langle \dot{\theta}_L^2 \rangle = b_0\, \epsilon_\theta/\tau_\eta$ and $\dot{\theta}_L = D_t\theta(\boldsymbol{x}_L(t),t)$ is the time derivative of a scalar along a fluid tracer. Also Eq. (6) captures very well the numerical simulations, at least for the explored case at $\mathrm{Sc} = 1$; see Fig. 2(b). We also note that for comparable values of v_s, the variance of the scalar time derivative, $\dot{\theta}_s$, is much larger than the variance of the fluid acceleration, seen in Fig. 2(a). By using (5) and (6) one can estimate the asymptotical relative increase factor as $\sim 3\mathrm{Sc}\, a_0/b_0$, which we evaluate to be ~ 13 at $\mathrm{Re}_\lambda = 75$ and ~ 17 at $\mathrm{Re}_\lambda = 125$. This difference in variances is likely to be originated by the presence of fronts (or ramp and cliffs [14]) in the spatial structure of the scalar field, sharper than the ones observed in a Cartesian component of the velocity; such fronts are crossed more and more as the probe propulsion is increased and greatly contribute to the scalar fluctuations.

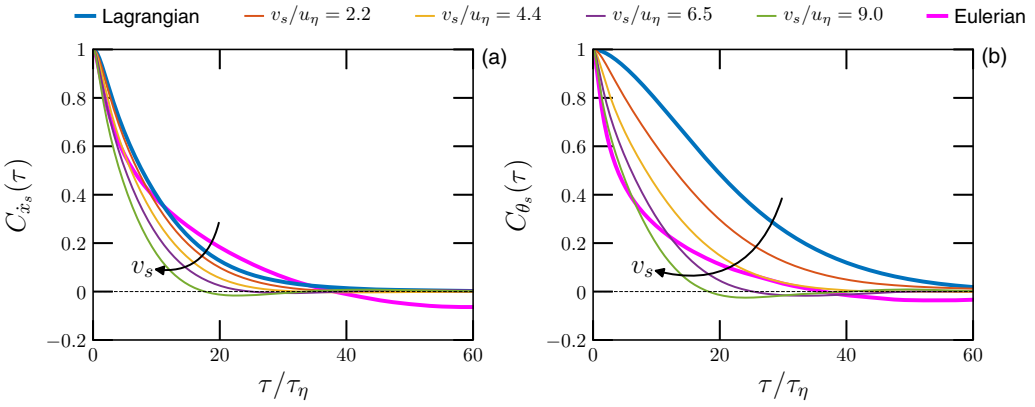

FIG. 3. (a) Behavior of the correlation function of the probe velocity $\dot{x}_{s,i}$ (single Cartesian component) and (b) correlation of the scalar value recorded by the probe θ_s at varying the transect velocity amplitude v_s (the arrows indicate its growing direction). The correlations functions computed from the fixed point, denoted as Eulerian, are also reported in both cases.

B. Two time statistics: Finite time gaps

We now look at the behavior of increments of the probe velocity and of the scalar field across finite-time gaps, and as before we aim at determining the trends as a function of the propulsion velocity. We initially examine the second-order statistics through correlation functions and spectra, while later higher-order moments will be investigated.

1. Correlation function and correlation time

We consider the temporal correlation functions of $\dot{x}_{s,i}(t)$ (meaning one Cartesian component) and $\theta_s(t)$ at varying v_s, whose measurements are reported in Fig. 3. From these graphs it is evident that, as the propulsion velocity is increased, both the velocity and scalar signal become less and less correlated. However, the limiting correlations function at large v_s significantly differs from the one that we measure for fixed-point (Eulerian) probes. Furthermore, the scalar signal in the Lagrangian frame is much more correlated then the single component of the velocity.

The observed trends in the correlation time can be understood by means of an approximate model. The starting point is again Eq. (4), which is used in the following to build an approximation for velocity increments and later for the correlations functions. When this equation is rephrased in terms of small but finite increments, τ for time and $\boldsymbol{v}_s\tau$ for space, it yields

$$\frac{\dot{\boldsymbol{x}}_s(\tau+t)-\dot{\boldsymbol{x}}_s(t)}{\tau} \simeq \frac{\boldsymbol{u}(\boldsymbol{x}_s(t)+\boldsymbol{x}_L(\tau),t+\tau)-\boldsymbol{u}(\boldsymbol{x}_s(t),t)}{\tau} + v_{s,j}\frac{\boldsymbol{u}(\boldsymbol{x}_s(t)+\boldsymbol{v}_s\tau,t)-\boldsymbol{u}(\boldsymbol{x}_s(t),t)}{v_{s,j}\,\tau} \tag{7}$$

with summation over j here implied. Note that $\boldsymbol{x}_L(\tau)$ denotes the position at time $t+\tau$ of a fluid tracer that was at the same position of the probe at time t. This simplifies to

$$\delta_\tau \dot{\boldsymbol{x}}_s \simeq \delta^L_\tau \boldsymbol{u} + \delta^E_{\boldsymbol{v}_s\tau}\boldsymbol{u}, \tag{8}$$

where we have introduced, respectively, (1) the temporal increment of the probe velocity, $\delta_\tau \dot{\boldsymbol{x}}_s = \dot{\boldsymbol{x}}_s(\tau+t)-\dot{\boldsymbol{x}}_s(t)$; (2) the velocity difference along the trajectory of a fluid tracer, $\delta^L_\tau \boldsymbol{u}(\boldsymbol{x}_s(t),t) \equiv \boldsymbol{u}(\boldsymbol{x}_s(t)+\boldsymbol{x}_L(\tau),t+\tau)-\boldsymbol{u}(\boldsymbol{x}_s(t),t)$, which is called Lagrangian velocity difference; and (3) the velocity difference across two positions in space at distance $\boldsymbol{l}$ and at a fixed time, $\delta^E_{\boldsymbol{l}}\boldsymbol{u}(\boldsymbol{x}_s(t),t) \equiv \boldsymbol{u}(\boldsymbol{x}_s(t)+\boldsymbol{l},t)-\boldsymbol{u}(\boldsymbol{x}_r(t),t)$, which we call Eulerian difference. If the two right-hand-side terms in (8) are taken as independent, this suggest that in statistically stationary conditions and for a single

Cartesian components, one has

$$\langle(\delta_\tau \dot{x}_{s,i})^2\rangle(\tau) \simeq \langle(\delta^L_\tau u_i)^2\rangle(\tau) + \left\langle\left(\delta^E_{\boldsymbol{v}_s\tau} u_i\right)^2\right\rangle(v_s\tau). \tag{9}$$

Note that due to isotropy and homogeneity the only dependencies left in the above term are in respect to time τ and to the amplitude of the displacement $v_s\tau$. In the limit $v_s \to 0$ the relation gives the fluid tracer (or Lagrangian) limit, while in the opposite asymptote $v_s \to +\infty$ it says that the spatial (Eulerian) increment will dominate. A final caveat should be added concerning the Eulerian increments $\delta^E_{\boldsymbol{v}_s\tau}\boldsymbol{u}$, which are neither longitudinal or transverse ones but rather a mixture of the two.[1]

The definition of the correlation function in term of the variance of increments, $C_{\boldsymbol{u}}(\tau) = 1 - \langle(\delta_\tau u_i)^2\rangle/(2\langle u_i^2\rangle)$, allows us to immediately recast Eq. (9) in term of correlations: $C_{\dot{x}_s}(\tau) \simeq C^E_{\boldsymbol{u}}(\boldsymbol{v}_s\tau) + C^L_{\boldsymbol{u}}(\tau) - 1$. The correlation time T_h for $\dot{x}_{s,i}$ can be defined as the time at which its correlation function decreases to a value h ($0 \leqslant h < 1$), and when the values of h is sufficiently close to 1, one can adopt a quadratic approximation for the Eulerian and Lagrangian correlation functions:

$$C^E_{\boldsymbol{u}}(\boldsymbol{v}_s\tau) \simeq 1 - \frac{(\boldsymbol{v}_s\tau)^2}{\tilde{\lambda}^2}, \qquad C^L_{\boldsymbol{u}}(\tau) \simeq 1 - \frac{\tau^2}{\tilde{\tau}^2_\lambda}. \tag{10}$$

The length $\tilde{\lambda}$ and time $\tilde{\tau}_\lambda$ are parameters which in the limit of vanishing τ become equal to the Taylor microscale of turbulence (λ) and to its temporal equivalent in the Lagrangian frame (denoted τ_λ). Finally, combining these all we reach the expression for the correlation time that can be tested on the numerical results:

$$T_C(v_s) = \sqrt{\frac{(1-C)}{\frac{v_s^2}{\tilde{\lambda}^2} + \frac{1}{\tilde{\tau}^2_\lambda}}}. \tag{11}$$

This correlation time is a decreasing function of v_s which vanishes in the limit of $v_s \to +\infty$; such a limit corresponds, however, to a finite correlation length $v_s \cdot T_C(v_s)$ by virtue of the Taylor frozen flow hypothesis, which becomes fully valid for large v_s. We note that a similar argument as the one proposed for the correlation of the probe velocity can be put forward for the scalar correlation time measured by the probe, after assuming that $\langle(\delta_\tau\theta_s)^2\rangle \simeq \langle(\delta^L_\tau\theta)^2\rangle(\tau) + \langle(\delta^E_{\boldsymbol{v}_s\tau}\theta)^2\rangle(v_s\tau)$. Figure 4 shows the so-called width-at-half-height correlation time, $T_{C=0.5}$, which corresponds to taking the value $C = 0.5$, in other words the time at which the correlation function has decreased from 1 to the value 1/2. It is shown that Eq. (11) well captures the behavior of $T_{C=0.5}$ as a function of v_s, when the free parameters $\lambda_{u,\theta}$ and $\tau_{\lambda_u,\lambda_\theta}$ are tuned. It is remarkable that the value for λ is similar in the case of scalar and velocity, and it is close to the value of the Taylor scale. We finally remark that the measurements of the correlation time performed by the fixed point probes appear difficult to connect to the correlation times evaluated on all the other probes. We suggest that the time-difference measurements performed in such a frame are strongly affected by the large flow structure of the flow and do not lead to a representative timescale for the flow [15].

2. Velocity and scalar energy spectra

We now look at the energy spectra. Despite the fact that such a quantity is closely related to the correlation function, being just proportional to its Fourier transform, it allows us to better highlight the scaling behavior of the kinetic energy, particularly with respect to the time frequency ω in the inertial range of scales $1/T_e \ll \omega \ll 1/\tau_\eta$. Indeed, on the basis of dimensional arguments one expects that in the inertial range for the Lagrangian limiting case, $E^L_{\boldsymbol{u}}(\omega) \sim \omega^{-2}$, while for the

[1]The second-order moment of the single-component Eulerian increment can be rewritten in the form $\langle(\delta^E_{\boldsymbol{v}_s\tau} u_i)^2\rangle = \langle(\delta^E_{\boldsymbol{v}_s\tau\parallel} u)^2\rangle + \langle(\delta^E_{\boldsymbol{v}_s\tau\perp} u)^2\rangle$ if the assumption is made that the longitudinal contribution, $\delta^E_{\boldsymbol{v}_s\tau\parallel} u \equiv \delta^E_{\boldsymbol{v}_s\tau}\boldsymbol{u} \cdot \boldsymbol{v}_s/|\boldsymbol{v}_s|$, and the transverse one, $\delta^E_{\boldsymbol{v}_s\tau\perp} u \equiv \delta^E_{\boldsymbol{v}_s\tau}\boldsymbol{u} \times \boldsymbol{v}_s/|\boldsymbol{v}_s|$, are statistically independent.

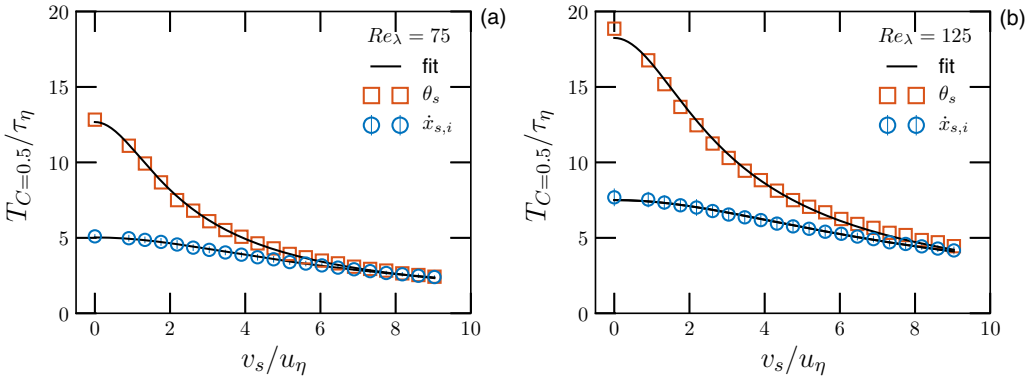

FIG. 4. Velocity and scalar correlation time, defined as width-at-half-height $T_{C=0.5}$, at varying the probe drifting velocity intensity v_s. Panel (a) reports results at $\mathrm{Re}_\lambda = 75$, and panel (b) at $\mathrm{Re}_\lambda = 125$. All measurements are well described by Eq. (11) with fitting parameters $\tilde{\tau}_\lambda = 7.1\tau_\eta(10.6\tau_\eta)$, $\tilde{\lambda} = 34.4\eta(62.4\eta)$ for the velocity, and $\tilde{\tau}_\lambda = 17.9\tau_\eta(25.8\tau_\eta)$, $\tilde{\lambda} = 30.3\eta(55.3\eta)$ for the scalar at $\mathrm{Re}_\lambda = 75(125)$.

Eulerian one, $E^E_{\boldsymbol{u}}(\omega) \sim \omega^{-5/3}$ [16,17]. The same is expected for the scalar energy spectra, $E_\theta(\omega)$, in the corresponding inertial range $1/T_\theta \ll \omega \ll 1/\tau_{\eta,\theta}$ [16,18]. It follows that spectra corresponding to intermediate v_s should fall between these two scaling behaviors. Our measurements for a selected number of probe speeds are shown in Fig. 5. First, we see that the Lagrangian measurements give spectra which are steeper than the Eulerian fixed-probe counterpart. The Lagrangian spectra agree with similar previous measurements, showing limited scaling ranges [19]. As the probe velocity is increased, for both velocity and scalar, we observe more gentle slopes. The $-5/3$ Kolmogorov scaling becomes particularly evident, in the range $\omega \simeq [0.01,0.1]\tau_\eta^{-1}$, for the probes that have a large propulsion velocity. The progressive shift from temporally dominated to spatially dominated scalings at increasing the probe speed as has been long known in the experimental domain and is often indicated as "flying hot-wire effect" [20]. However, it is remarkable here that already for drifting probes at $v_s = 9u_\eta \simeq u_{\mathrm{rms}}$ the frozen flow approximation becomes fully valid and leads to very neat $\omega^{-5/3}$ scalings. Such a scaling is much clearer than the one observed for the fixed probe. It is indeed known that in turbulent flows that do not possess a mean flow, the spectra measured in a time domain from a fixed probe (Eulerian measurement) give results different from the expected ones (i.e., from the $-5/3$ scaling). In the condition of no-mean flow, indeed, the Taylor frozen flow hypothesis cannot be applied, and the resulting temporal spectra may be affected by the persistence of large-scale structures in the flow, as pointed out in Ref. [21]. We further observe that the scalar spectra for Lagrangian tracers appear to be rather different from the corresponding velocity one. The region compatible with a ω^{-2} scaling is confined to very large scales, while the rest of the spectra appear to better agree with a ω^{-3} behavior. We attribute this feature to the limited Péclet number of our simulations, which are consistent with the numerical results by Yeung [22] at similar Péclet and Schmidt values. The ω^{-3} scaling can indeed be obtained by assuming that the scalar variations along a Lagrangian trajectory are smooth, in other words, dominated by the diffusion process. This is the counterpart of the observation that the scalar is much more correlated in time as compared to the single component of the velocity field. The steep scaling of the Lagrangian scalar spectra, estimated as $\omega^{-8/3}$, was also observed in the mentioned simulations [22] and was seen to decrease when increasing the turbulence intensity. Finally, also for the case of scalar measurements, we observe that the fixed point spectra do not give consistent results with the $-5/3$ scaling, while the scaling for highly propulsive probes ($v_s \simeq u_{\mathrm{rms}}$) is much closer to the expected Obhukhov-Corrsin phenomenology [18].

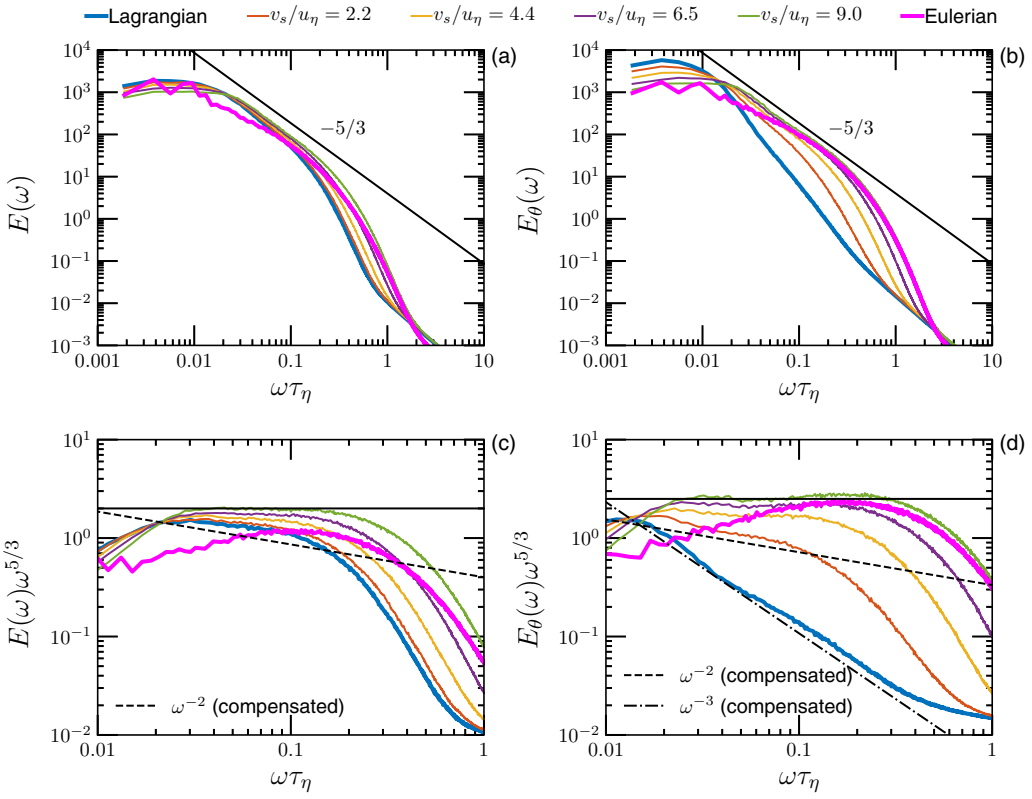

FIG. 5. Spectra of kinetic energy (a) and passive scalar field spectra (b) at $\mathrm{Re}_\lambda \simeq 125$. The compensated spectra with respect to $\omega^{-5/3}$ are reported in panels (c) and (d). The power-law scalings $\omega^{-5/3}$, ω^{-2}, corresponding respectively to turbulence in Eulerian frame or Lagrangian frame and the dissipative scaling and ω^{-3}, are reported. Note the so-called "flying hot-wire effect": the progressive shift from Lagrangian to Eulerian scalings at increasing v_s: at $v_s \simeq u_{\mathrm{rms}}$ the frozen flow approximation becomes fully valid and leads to clean $\omega^{-5/3}$ scalings.

3. High-order statistical moments of velocity and scalar increments

How are higher statistical moments of velocity and scalar time differences affected by the propulsion velocity? In order to clarify this point we focus on the flatness of such quantities as a function of the time gap τ:

$$\mathcal{F}(\tau) = \frac{\langle (\delta_\tau \dot{x}_{s,i})^4 \rangle}{\langle (\delta_\tau \dot{x}_{s,i})^2 \rangle^2}, \quad \mathcal{F}_\theta(\tau) = \frac{\langle (\delta_\tau \theta)^4 \rangle}{\langle (\delta_\tau \theta)^2 \rangle^2}, \tag{12}$$

and we compute them for different propulsion velocities [note that the summation over the index i is not implied in Eq. (12)]. We begin by looking at the behavior of the velocity field, Fig. 6(a). For small gaps and zero propulsion velocity the flatness is at its maximum (it is about 18 at $\mathrm{Re}_\lambda = 125$). We note that the vanishing time-gap limit corresponds to the flatness of the probe acceleration, $\mathcal{F}_a$, which is shown in the inset of the figure. The latter quantity for increasing v_s samples mostly the statistics of the velocity field, and in the asymptotic limit ($v_s \to +\infty$) one can estimate that it will reach the plateau $\mathcal{F}_a = 3/25\, \mathcal{F}_{\partial_\parallel u_i} + 24/25\, \mathcal{F}_{\partial_\perp u_i}$ (demonstration in Supplemental Material [10]; see also Refs. [23,24]), a prediction which is consistent with our simulations (see again the inset). When the time gaps τ are increased, all the curves monotonically decrease to the Gaussian value ($\mathcal{F} = 3$). Similarly to the trends observed for the limit $\tau \to 0$, we can also observe that the increase of the propulsion velocities v_s produces a progressive reduction in the flatness. For the largest velocities we

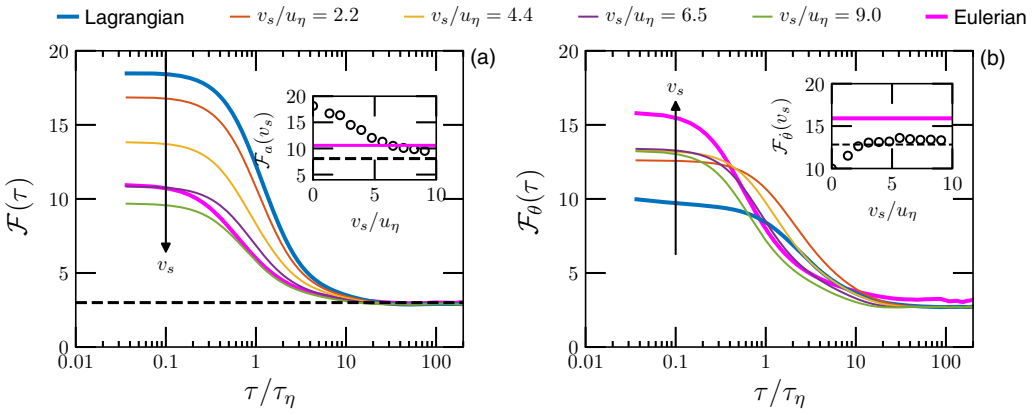

FIG. 6. (a) Flatness of probe velocity time increments $\mathcal{F}_{\delta_\tau \dot{x}_{s,i}}$ as a function of the increment τ for different probes' velocity amplitudes v_s. The horizontal dashed line indicates the flatness value of a Gaussian random variable $\mathcal{F} = 3$. In the inset the behavior of the same quantity in the vanishing time-gap limit, $\mathcal{F}_a$ is shown. The horizontal dashed line shows the asymptotic ($v_s \to +\infty$) prediction $\mathcal{F}_a = 3/25\ \mathcal{F}_{\partial_\parallel u_i} + 24/25\ \mathcal{F}_{\partial_\perp u_i}$. (b) Flatness of scalar time increments $\mathcal{F}_\theta$. The inset shows the behavior of the same quantity in the vanishing time-gap limit, $\mathcal{F}_{\dot\theta}$. The dashed line gives the expected asymptotic limit $\mathcal{F}_{\dot\theta} = \mathcal{F}_{\partial\theta}$. In both panels the arrows denote the trend at increasing the intensity of the propulsion velocity, v_s.

measure flatness values that at all time gaps τ are close to the ones that are detected in the Eulerian fixed-point system, meaning probably that relative higher-order statistics are less affected by the spurious effects introduced by the absence of a mean flow.

We now turn our attention to the scalar time-increments flatness [Fig. 6(b)]. In the present analysis it appears that the most intermittent situation occurs again for small time gaps, although in this case for the highly movable probes ($v_s = 9u_\eta \simeq u_{\rm rms}$). This is confirmed by the inset, where the vanishing time limit is shown as $\mathcal{F}_{\dot\theta}$, together with the asymptotic ($v_s \to +\infty$) prediction $\mathcal{F}_{\dot\theta} = \mathcal{F}_{\partial\theta}$. Contrary to what happens to the velocity, we note that we obtain here a reduced flatnesses for decreasing values of the probe speed, with a minimum occurring in the Lagrangian case [note the arrows directions in Figs. 6(a) and 6(b)]. The low intermittent level of Lagrangian scalar time increments already has been observed by Bec *et al.* [25]. In the large gap limit we do not exactly find the Gaussian flatness value for the probes, but rather a weakly sub-Gaussian one ($\sim$2.7). This points to long-range correlations which seem to be nondetectable in the fixed-position probe system. Finally, note that in all cases the scalar is less intermittent than the velocity field.

To have a deeper understanding on the scaling behavior as a function of the time gap, in Fig. 7 we plot the local slopes by using extended self-similarity (ESS), i.e., the logarithmic derivative of the fourth-order temporal structure function, $\langle(\delta_\tau \dot{x}_{s,i})^4\rangle$, versus the second-order one, $\langle(\delta_\tau \dot{x}_{s,i})^2\rangle$, which gives [26]

$$\zeta_{4,2}(\tau) = \frac{d\log\langle(\delta_\tau \dot{x}_{s,i})^4\rangle}{d\log\langle(\delta_\tau \dot{x}_{s,i})^2\rangle}, \quad \zeta^\theta_{4,2}(\tau) = \frac{d\log\langle(\delta_\tau \theta)^4\rangle}{d\log\langle(\delta_\tau \theta)^2\rangle}. \tag{13}$$

This quantity is a direct scale-by-scale measurement of the local scaling properties. A scale-independent behavior of the fourth moment against the second-order one would result in a constant value for the left-hand side of (13). Furthermore, in the absence of intermittency, these curves would be constant across the time lags with $\zeta_{4,2}(\tau) = \zeta^\theta_{4,2}(\tau) = 2$. While the latter relation is always well verified for the smooth dissipative scales ($\tau < 0.1\tau_\eta$), a nontrivial behavior appears in the inertial range, illustrating the intermittent feature of the turbulent flow. In the time range from 1 to 10 in τ_η units, the strong deviation observed in the local slope for the velocity has been attributed to events of tracer trapping in intense vortex filaments [27]. We observe that these events tend to fade out as

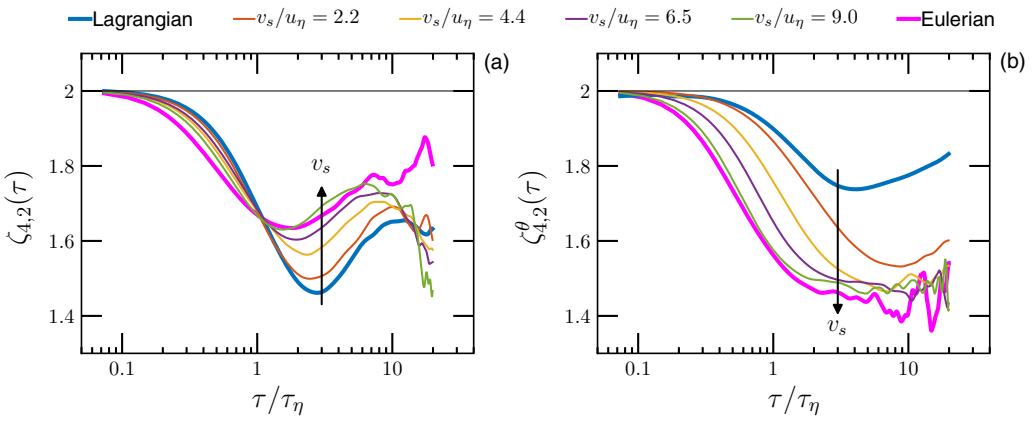

FIG. 7. (a) ESS local slopes, i.e., logarithmic derivative of the fourth-order moments of probe velocity time increments versus the second-order one as in Eq. (13). (b) Same as before for scalar increments. Note the opposite intermittency trends between the velocity and the scalar at increasing v_s intensity (arrow direction).

soon as v_s is increased, indicating that fast enough probes can escape from such filaments. However, it is interesting to observe that the deepening associated with this highly intermittent range seems to remain for the case of the highest propulsion velocities and to be close, if not coincident, to the level of intermittency measured in the Eulerian fixed-point probe. This observation questions the vortex-filament interpretation of the so-called bottleneck effect [28]. The behavior of the scalar [Fig. 7(b)] deserves further attention. First, we observe that the scalar is highly intermittent both in the fixed-position frame and in the fast drifting one. The values of the exponent we detect here are as low as 1.5 ± 0.1, and this all the way above time gaps $\tau \gtrsim 1\tau_\eta$. Such a strongly intermittent behavior has been known for a long time [29], and it has been associated with the presence of scalar sharp fronts. When decreasing the propulsion velocity we observe many fewer intermittent fluctuations till reaching, at $v_s = 0$, the Lagrangian case that is by far the less intermittent case (with $\zeta^\theta_{4,2}(\tau) \sim 1.8$), although a clear inertial range plateau cannot be attained in the present simulations.

IV. CONCLUSIONS

We have performed a numerical study of the statistical properties of fluid velocity and scalar concentration fields as measured by small ideal propelled probes in a turbulent flow environment. It has been highlighted that despite the simplicity of the model system taken into consideration, the properties of the recorded signals are far from being trivial because they mix Lagrangian and Eulerian turbulent statistical properties. We have first focused on time derivatives of velocity (so acceleration) and scalar concentrations. It appears that, as the propulsion velocity is increased, the probe samples more and more the spatial gradient properties of the fields, and we have predicted that such a behavior evolves quadratically with the ratio of the propulsion speed intensity over the Kolmogorov velocity v_s/u_η, with a weak Reynolds number, Péclet number dependencies parametrized by the Heisenberg-Yaglom coefficient, a_0, and its scalar equivalent, b_0. Such an increase of variance with the propulsion speed is remarkably larger for the scalar as compared to the fluid velocity field, and it signals the higher spatial variations of the scalar field. Our analysis of finite time increments of fluid velocity and of the scalar encompasses the correlation functions and correlation time, for which an empirical model has been proposed, and the Fourier spectra. It is worth noticing that this analysis demonstrates that probes with a propulsive speed of the order of the turbulent root-mean-square velocity fluctuation, $v_s \simeq u_{\rm rms}$, already display nearly straight line trajectories and can be considered good tools to measure the Eulerian properties of the flow. Indeed, measurements in such conditions reveal the expected $-5/3$ scaling both for velocity and for the scalar in a much clearer way than for the

fixed-point measurements where, due to the absence of mean flow, the Taylor frozen-flow hypothesis fails. The two-point higher-order statistics highlight in a striking way the opposite trends displayed by the velocity and scalar fields. While the velocity field in the Lagrangian frame is characterized by wide fluctuations and so by stronger intermittent scaling properties as compared to the Eulerian one, the reverse is true for the scalar. In our opinion it remains to be verified if the origin of such differences is originated by the presence of rather different coherent structures, namely, vortex filaments for the fluid and ramp-cliff fronts for the scalar.

Finally, we would like to readdress the applicative questions that originally motivated this study: the consequence for AUVs or boats drifting in turbulent ocean. From the above discussion it is clear that two relevant velocity scales are at play: u_η and $u_{\rm rms}$. While the former has a role in the description of the time-derivatives statistics of the measured fields, the latter is important for finite-time gaps observables and spectra. Such scales in the upper ocean have been estimated to be of the order $O(1)$ cm/s and $O(10)$ cm/s, respectively [30–32]. This implies that the most common AUV systems, which typically propel at much larger velocities, $O(1)$ m/s [31], will effectively probe frozen flow turbulent properties (e.g., for spectra or structure functions), while miniaturized versions, μAUVs, which have less power and so smaller propulsive force, might find themselves in a transitional Lagrangian or Eulerian measurements regime. However, the probe model system adopted in our study is still rather simplistic because it neglects, among other effects, the probe inertia, the hydrodynamic drag, and the buoyancy force. The shape of the probe may also have a crucial role, since it can affect the hydrodynamic torque due to the surrounding flow. These are still open points which need to be addressed in future work. We conclude by observing that not only is this study relevant for the domain of measurements in the ocean, but it can also be suitable for the description of the perceived fields by small swimming organisms attracted by a given point or direction in space. Indeed, similar modeling has been adopted for recent studies of swimming phototactic algae or bacteria in turbulent [33] and chaotic flow environments [34].

ACKNOWLEDGMENTS

The present study has been supported by the Sino-French (NSFC-CNRS) joint project (No. 11611130099, NSFC China; PRC 2016-2018 LATUMAR, Lagrangian turbulence: Numerical studies and marine experimental applications, CNRS France). Y.H. is partially supported by the National Natural Science Foundation of China (Grants No. 11332006 and 11732010).

[1] H. L. Grant, R. W. Stewart, and A. Moilliet, Turbulence spectra from a tidal channel, J. Fluid Mech. **12**, 241 (1962).

[2] R. B. Wynn, V. A. I. Huvenne, T. P. Le Bas, B. J. Murton, D. P. Connelly, B. J. Bett, H. A. Ruhl, K. J. Morris, J. Peakall, D. R. Parsons, E. J. Sumner, S. E. Darby, R. M. Dorrell, and J. E. Hunt, Autonomous underwater vehicles (AUVs): Their past, present and future contributions to the advancement of marine geoscience, Marine Geol. **352**, 451 (2014).

[3] M. J. Perry and D. L. Rudnick, Observing the ocean with autonomous and Lagrangian platforms and sensors: The role of ALPS in sustained ocean observing systems, Oceanography **16**, 31 (2003).

[4] D. Walker, Micro autonomous underwater vehicle concept for distributed data collection, in *Oceans 2006* (IEEE, 2006), pp. 1–4.

[5] S. A. Watson, D. J. P. Crutchley, and P. N. Green, The mechatronic design of a microautonomous underwater vehicle (μAUV), Int. J. Mech. Autom. **2**, 157 (2012).

[6] J. S. Jaffe, P. J. S. Franks, P. L. D. Roberts, D. Mirza, C. Schurgers, R. Kastner, and A. Boch, A swarm of autonomous miniature underwater robot drifters for exploring submesoscale ocean dynamics, Nat. Commun. **8**, 14189 (2017).

[7] T. R. Osborn and R. G. Lueck, Turbulence measurements from a towed body, J. Atmos. Ocean. Technol. **2**, 517 (1985).
[8] X. Shan, Simulation of Rayleigh-Bénard convection using a lattice Boltzmann method, Phys. Rev. E **55**, 2780 (1997).
[9] P. Perlekar, L. Biferale, M. Sbragaglia, S. Srivastava, and F. Toschi, Droplet size distribution in homogeneous isotropic turbulence, Phys. Fluids **24**, 065101 (2012).
[10] See Supplemental Material at http://link.aps.org/supplemental/10.1103/PhysRevFluids.3.054604 for further details on numerical simulations and their validation and for the derivation of single-point statistical relations for the fluid velocity and scalar field.
[11] V. Mathai, E. Calzavarini, J. Brons, C. Sun, and D. Lohse, Microbubbles and Microparticles are Not Faithful Tracers of Turbulent Acceleration, Phys. Rev. Lett. **117**, 024501 (2016).
[12] G. A. Voth, A. La Porta, A. M. Crawford, J. Alexander, and E. Bodenschatz, Measurement of particle accelerations in fully developed turbulence, J. Fluid Mech. **469**, 121 (2002).
[13] J. K. Zbrozek, Some effects of atmospheric turbulence on aircraft, Weather **13**, 215 (1958).
[14] Z. Warhaft, Passive scalars in turbulent flows, Annu. Rev. Fluid Mech. **32**, 203 (2000).
[15] L. Biferale, E. Calzavarini, and F. Toschi, Multi-time multi-scale correlation functions in hydrodynamic turbulence, Phys. Fluids **23**, 085107 (2011).
[16] H. Tennekes and J.L. Lumley, *A First Course in Turbulence* (MIT Press, Cambridge, MA, 1972).
[17] F. G. Schmitt and Y. Huang, *Stochastic Analysis of Scaling Time Series: From Turbulence Theory to Applications* (Cambridge University Press, Cambridge, 2016).
[18] Katepalli R. Sreenivasan, The passive scalar spectrum and the Obukhov-Corrsin constant, Phys. Fluids **8**, 189 (1996).
[19] Y. Huang, L. Biferale, E. Calzavarini, C. Sun, and F. Toschi, Lagrangian single-particle turbulent statistics through the Hilbert-Huang transform, Phys. Rev. E **87**, 041003 (2013).
[20] J. H. Watmuff, A. E. Perry, and M. S. Chong, A flying hot-wire system, Exp. Fluids **1**, 63 (1983).
[21] J.-F. Pinton and R. Labbé, Correction to the Taylor hypothesis in swirling flows, J. Phys. II **4**, 1461 (1994).
[22] P. K. Yeung, Lagrangian characteristics of turbulence and scalar transport in direct numerical simulations, J. Fluid Mech. **427**, 241 (2001).
[23] L. Fang, Y. J. Zhang, J. Fang, and Y. Zhu, Relation of the fourth-order statistical invariants of velocity gradient tensor in isotropic turbulence, Phys. Rev. E **94**, 023114 (2016).
[24] T. Ishihra, Y. Kaneda, M. Yokokawa, K. Itakura, and A. Uno, Small-scale statistics in high-resolution direct numerical simulation of turbulence: Reynolds number dependence of one-point velocity gradient statistics, J. Fluid Mech. **592**, 335 (2007).
[25] J. Bec, H. Homann, and G. Krstulovic, Clustering, Fronts, and Heat Transfer in Turbulent Suspensions of Heavy Particles, Phys. Rev. Lett. **112**, 234503 (2014).
[26] A. Arnéodo, R. Benzi, J. Berg, L. Biferale, E. Bodenschatz *et al.*, Universal Intermittent Properties of Particle Trajectories in Highly Turbulent Flows, Phys. Rev. Lett. **100**, 254504 (2008).
[27] L. Biferale, G. Boffetta, A. Celani, A. Lanotte, and F. Toschi, Particle trapping in three-dimensional fully developed turbulence, Phys. Fluids **17**, 021701 (2005).
[28] M. Buzzicotti, A. Bhatnagar, L. Biferale, A. S. Lanotte, and S. S. Ray, Lagrangian statistics for Navier-Stokes turbulence under Fourier-mode reduction: Fractal and homogeneous decimations, New J. Phys. **18**, 113047 (2016).
[29] K. R. Sreenivasan and J. Schumacher, Lagrangian views on turbulent mixing of passive scalars, Philos. Trans. R. Soc. **368**, 1561 (2010).
[30] J. Jiménez, Oceanic turbulence at millimeter scales, Scientia Marina **61**, 47 (1997).
[31] S. A. Thorpe, *An Introduction to Ocean Turbulence* (Cambridge University Press, Cambridge, 2007).
[32] K. Korotenko, A. Sentchev, F. G. Schmitt, and N. Jouanneau, Variability of turbulent quantities in the tidal bottom boundary layer: Case study in the eastern English Channel, Continental Shelf Res. **58**, 21 (2013).
[33] C. Torney and Z. Neufeld, Phototactic Clustering of Swimming Microorganisms in a Turbulent Velocity Field, Phys. Rev. Lett. **101**, 078105 (2008).
[34] J. Dervaux, M. Capellazzi Resta, and P. Brunet, Light-controlled flows in active fluids, Nat. Phys. **13**, 306 (2017).